Effect of oxygen incorporation on the structure and elasticity of Ti-Al-O-N coatings synthesized by cathodic arc and high power pulsed magnetron sputtering

M. Hans, M. to Baben, D. Music, J. Ebenhöch, D. Primetzhofer, D. Kurapov, M. Arndt, H. Rudigier, and J. M. Schneider

Citation: Journal of Applied Physics **116**, 093515 (2014); doi: 10.1063/1.4894776
View online: http://dx.doi.org/10.1063/1.4894776
View Table of Contents: http://scitation.aip.org/content/aip/journal/jap/116/9?ver=pdfcov
Published by the AIP Publishing

Effect of oxygen incorporation on the structure and elasticity of Ti-Al-O-N coatings synthesized by cathodic arc and high power pulsed magnetron sputtering

M. Hans,[1,a)] M. to Baben,[1] D. Music,[1] J. Ebenhöch,[1] D. Primetzhofer,[2] D. Kurapov,[3] M. Arndt,[3] H. Rudigier,[3] and J. M. Schneider[1]
[1]*Materials Chemistry, RWTH Aachen University, Kopernikusstr. 10, D-52074 Aachen, Germany*
[2]*Department of Physics and Astronomy, Uppsala University, Lägerhyddsvägen 1, S-75120 Uppsala, Sweden*
[3]*Oerlikon Balzers Coating AG, Iramali 18, LI-9496 Balzers, Principality of Liechtenstein*

(Received 27 June 2014; accepted 25 August 2014; published online 5 September 2014)

Ti-Al-O-N coatings were synthesized by cathodic arc and high power pulsed magnetron sputtering. The chemical composition of the coatings was determined by means of elastic recoil detection analysis and energy dispersive X-ray spectroscopy. The effect of oxygen incorporation on the stress-free lattice parameters and Young's moduli of Ti-Al-O-N coatings was investigated by X-ray diffraction and nanoindentation, respectively. As nitrogen is substituted by oxygen, implications for the charge balance may be expected. A reduction in equilibrium volume with increasing O concentration is identified by X-ray diffraction and density functional theory calculations of Ti-Al-O-N supercells reveal the concomitant formation of metal vacancies. Hence, the oxygen incorporation-induced formation of metal vacancies enables charge balancing. Furthermore, nanoindentation experiments reveal a decrease in elastic modulus with increasing O concentration. Based on *ab initio* data, two causes can be identified for this: First, the metal vacancy-induced reduction in elasticity; and second, the formation of, compared to the corresponding metal nitride bonds, relatively weak Ti-O and Al-O bonds. © *2014 AIP Publishing LLC*.
[http://dx.doi.org/10.1063/1.4894776]

I. INTRODUCTION

It is well known that the incorporation of Al into NaCl-structured TiN (space group $Fm\bar{3}m$) results in an elevated oxidation resistance, e.g., up to 700 °C for a composition of $(Ti_{0.28}Al_{0.29})_{0.56}N_{0.44}$.[1] While the effects of substitutions on the metal sublattice of TiAlN-based coatings have been studied extensively in the past[2] (and references therein), very little is known about the effect of substitutions on the non-metal sublattice on the properties and performance of such coatings.

The effect of O incorporation into TiAlN-based coatings on the performance has been investigated for multilayer systems: TiAlN/TiAlON multilayers, deposited by magnetron sputter ion plating onto WC substrates, showed an improved wear behaviour in dry drilling of tempered steel, compared to monolithic TiAlN, which was attributed to be due to the increased oxidation resistance.[3] TiAlON/TiAlN/TiN multilayers, synthesized by plasma enhanced chemical vapor deposition onto steel substrates, showed no mass gain after exposure to air at 800 °C for 1 h and it has been concluded that oxidation was prevented at this temperature.[4] Furthermore, these multilayers were dipped into molten aluminium and the mass loss was compared to TiAlN/TiN: the oxynitride showed a factor two lower mass loss due to corrosion after 20 h immersion time.[4]

$(Ti_{0.35}Al_{0.65})(O_xN_{1-x})_y$ coatings were synthesized by reactive cathodic arc deposition by Sjölén *et al.*[5] They reported that oxygen incorporation affected the phase formation: while the coatings exhibited cubic structure for an $O/(O+N)$ ratio < 0.15 (corresponding to an O concentration of approximately 7.5 at. %), the growth of an amorphous phase on top of the cubic layer was observed for $0.15 < O/(O+N)$ ratio < 0.5 by X-ray diffraction (XRD) and transmission electron microscopy.[5] While for arc-evaporated $Ti_{0.34}Al_{0.66}N$ coatings hardness values of $H = 33 \pm 1$ GPa (Ref. 6) were reported, the oxynitrides with $O/(O+N)$ ratios > 0.15 exhibited with < 22 GPa significantly smaller hardness values. This was suggested to be due to grain boundary sliding within the nanocomposite, consisting of cubic and amorphous phase, however, there is no direct experimental evidence presented.[5]

Lattice parameters and bulk modulus values of $Ti_{0.5}Al_{0.5}N_{1-x}O_x$ supercells were predicted by density functional theory (DFT) calculations to increase by 0.7% and decrease by 19%, respectively, as x is increased from 0 to 0.5.[7] At this point, there is no experimental stress-free lattice parameter data for the Ti-Al-O-N system available in literature. The O concentration-induced reduction in bulk modulus was suggested to be due to a concomitant increase in metallic bonding character at the expense of covalent bonding.[7] A systematic DFT study on $M_{0.5}Al_{0.5}N_{1-x}O_x$ ($M = Sc$, Ti, V, Cr) revealed that the addition of oxygen leads to a significant reduction in bulk modulus, independent of transition metal M, due to formation of relatively long and, hence, weak M-O bonds.[8] It has been confirmed that this physical mechanism[7] is

[a)]Author to whom correspondence should be addressed. Electronic mail: hans@mch.rwth-aachen.de

relevant for $M_{0.5}Al_{0.5}N_{1-x}O_x$ (M = Sc, Ti, V, Cr)[8] and likely pertains to cubic transition metal aluminium oxynitrides in general. Furthermore, these predictions are consistent with experimental data for M = Cr, V: $Cr_{0.5}Al_{0.5}N$ and $(Cr_{0.45}Al_{0.55})_{0.38}(O_{0.97}N_{0.03})_{0.62}$ exhibited Young's modulus values of approximately 420 and 310 GPa, respectively,[9] while $(V_{0.5}Al_{0.5})_{0.48}N_{0.52}$ and $(V_{0.5}Al_{0.5})_{0.48}(O_{0.77}N_{0.23})_{0.52}$ showed values of approximately 370 and 230 GPa, respectively.[10]

Contradictory to these reports, experimental data on the elasticity of reactively magnetron sputtered, cubic-structured (Ti,Al)(O,N) coatings showed an increasing Young's modulus value from approximately 390 to 420 GPa for increasing O concentration from 0 to 20 at. %.[11] Moreover, the Young's modulus values of reactive cathodic arc-deposited cubic-structured CrO_xN_{1-x} with x in the range of 0 to 0.7 were measured to be 325 ± 25 GPa.[12]

From a crystal chemistry point of view, the substitution of nitrogen by oxygen has implications for the charge balance: according to Pauling's rules, stable ionic structures must preserve local electroneutrality.[13] It was previously shown that electroneutrality governs the incorporation of hydrogen into strontium titanate at growth temperatures of ≤200 °C (Ref. 14); and for perovskite oxynitrides, it has been argued that the following defect scenarios may be relevant: formation of anion vacancies, substitution within the anionic or cationic sublattice and cation oxidation.[15] Also for wurtzite, spinel, fluorite, and pyrochlore oxynitrides, the substitution within the anionic or cationic sublattice seems to stabilize these structures.[16] Based on formal charge state considerations and the comparison between *ab initio* and XRD data, the formation of metal vacancies was reported in the system Al-Si-N as Al (+3) is substituted by Si (+4).[17,18] The following scenarios are discussed in the literature for cubic transition metal oxynitrides: the formation of excess anion interstitials[7,9] or the formation of cation vacancies.[7,9,12,19,20] However, no conclusive evidence for any of the above mentioned scenarios could be found in the published literature until Shaha *et al*. reported, based on a comparative analysis of *ab initio* and XRD data, that metal vacancies form as nitrogen is substituted by oxygen in $V_{0.5}Al_{0.5}O_xN_{1-x}$.[10] The formation of metal vacancies enables charge neutrality of the formed oxynitride compounds. It is unclear at this point, whether the oxygen-induced formation of metal vacancies, as apparent in V-Al-O-N, is a general characteristic of cubic transition metal aluminium oxynitrides.

The above cited papers, addressing the composition dependence of transition metal (aluminium) oxynitride coatings, may be summarized as follows: Predictions regarding the compositional dependence of the elastic properties[7,8] are in part consistent with experiments,[9,10] but also in conflict with several reports.[11,12] The reasons for these inconsistencies have not been addressed in the literature. It is also evident that the calculated lattice parameters obtained from $V_{0.5}Al_{0.5}O_xN_{1-x}$ supercells with sufficient metal vacancy concentrations to enable charge neutrality show excellent agreement with the XRD data of high power pulsed magnetron sputtered (HPPMS) thin films.[10] Although Ti-Al-O-N coatings have been synthesized, no experimental stress-free lattice parameters were reported.

Our goal in the present study is to contribute towards understanding the effect of oxygen incorporation on the structure and elasticity in Ti-Al-O-N coatings and, by comparison with previously published predictions by Rotert *et al*.[8] and Shaha *et al*.,[10] assess the general relevance thereof. We report stress-free lattice parameters and Young's modulus values as a function of O concentration in the coatings. Ti-Al-O-N coatings were deposited by cathodic arc and HPPMS to examine a possible influence of the deposition technique. Based on Shaha's proposal for the V-Al-O-N defect structure,[10] metal vacancy containing supercells were generated for Ti-Al-O-N and compared to the experimentally determined lattice parameter and Young's modulus data.

II. EXPERIMENTAL DETAILS

Ti-Al-O-N coatings were synthesized by cathodic arc deposition in an industrial deposition plant Ingenia P3e™ made by Oerlikon Balzers Coating AG. Prior to each deposition circular 23 mm in diameter 90MnCrV8 steel substrates were cleaned ultrasonically with acetone and methanol for 5 min and mounted onto a two-fold rotation carousel. When a base pressure $<3.0 \times 10^{-4}$ Pa was reached, the substrate was heated to 450 °C and cleaned by plasma etching in an Ar/H_2 atmosphere. A TiN interlayer was applied in order to improve adhesion of the Ti-Al-O-N coating. The Ti-Al-O-N coatings were deposited at varying O_2 flows from 0 to 70 sccm and N_2 flows from 590 to 530 sccm, while the total pressure was kept constant at 3.2 Pa. Alloyed TiAl targets with 50 at. % Al were used and the substrates were at floating potential. The experimental setup for HPPMS depositions can be found elsewhere.[21] Additional O_2 flows of 6, 7, and 10 sccm were employed in the present study.

The chemical composition of the Ti-Al-O-N coatings was measured by energy dispersive X-ray spectroscopy (EDX) in a JEOL JSM-6480 scanning electron microscope, equipped with an EDAX Genesis 2000 device, at 10 kV acceleration voltage. A $(Ti_{0.5}Al_{0.5})_{0.47}(O_{0.45}N_{0.55})_{0.53}$ film, measured by elastic recoil detection analysis (ERDA), served as standard for the EDX analysis.

Time-of-Flight Energy ERDA experiments were performed at the tandem accelerator laboratory at Uppsala University. Samples were transferred to a vacuum chamber at a base pressure $<1.0 \times 10^{-4}$ Pa. 36 MeV $^{127}I^{8+}$ ions were used as primary projectiles. The detection beam line was situated under an angle of 45° with respect to the primary beam, with both incidence and exit angle of beam and detected particles at 22.5° with respect to the surface. Further details on the detection systems can be found in Ref. 22. For the present choice of primary ion and energy, depth profiling of all elements up to a depth in the range of 200 to 300 nm was possible. Besides surface contaminations by hydrogen, oxygen, and carbon, the investigated sample exhibited homogeneous depth profile within the above stated limits. Evaluation of time-energy coincidence spectra of recoils was done using the CONTES program package.[23]

Structural analysis was performed by XRD in a Siemens D5000 system with Bragg-Brentano geometry. The 2θ range of 30° to 80° was scanned with a step size and scan time per

step of 0.05° and 4 s, respectively. Stress-free lattice parameters were obtained according to the method of Genzel for ⟨001⟩ textured cubic crystals[24] from XRD analysis in a Bruker AXS D8 Discover General Area Diffraction Detection System. (111), (200), and (220) lattice planes were measured in Bragg-Brentano geometry at sample tilting angles of 36°, 0°, and 45° respective to the surface normal. Under this condition, the strain ε_{hkl} can be determined by[24]

$$\varepsilon_{hkl} = \left(2s_{12} + (s_{11} - s_{12})\frac{h^2 + k^2}{h^2 + k^2 + l^2}\right)\sigma,$$

whereas σ denotes residual stress and h, k, and l are the miller indices. The elastic compliances s_{ij} were taken from Ref. 25 and the stress-free lattice parameter a_0 was obtained according to

$$a_{hkl} = a_0\varepsilon_{hkl} + a_0,$$

and a_{hkl} is the lattice parameter measured for the corresponding (hkl) lattice plane. The Cu Kα sources were operated at 40 kV acceleration voltage and 40 mA current in all XRD measurements.

The average surface roughness of the thin films was measured by optical laser microscopy with a Keyence VK-9700 system with a 150X magnification objective lens.

Young's modulus of the coatings was determined by nanoindentation in a Hysitron TI-900 TriboIndenter by the method of Oliver and Pharr.[26] The indentations were performed load-controlled with a diamond Berkovich tip and the maximum load was 10 mN. The indentation depth was below 10% of the film thickness to avoid any substrate influence. For the cathodic arc coatings, 45 individual load-displacement curves were recorded for each sample; while for HPPMS coatings, 16 indents per sample were performed and averaged. Fused silica was used to derive and confirm the tip area function before and after each sample. The measured reduced modulus was calculated and converted into Young's modulus of the samples E_S by using the Poisson's ratio of $\nu_S = 0.214$, which is assumed to be independent of composition.[27]

III. COMPUTATIONAL DETAILS

DFT calculations[28] were performed with the Vienna *ab initio* simulation package. The general gradient approximation[29] was used for the exchange energy with an energy cut-off of 500 eV. The relaxation convergence was 10^{-3} eV and a Monkhorst-Pack k-point mesh of $6 \times 6 \times 6$ served for Brillouin-zone integration.[30] The total energy was modified by means of the tetrahedron method with Blöchl-corrections.[31] The $2 \times 2 \times 2$ supercell with 64 atoms was adopted from the C#3 configuration by Mayrhofer *et al.* and this configuration exhibits high stability due to minimum number of Ti-Al bonds.[32] The N and O atoms were distributed by special quasi-random structures[33] on the non-metal sublattice. Due to the complexity of modelling disorder effects in multi-sublattice systems, correlations between atoms on different sublattices were not investigated here. The equilibrium bulk moduli and lattice parameters of the metastable $Ti_{0.5-\delta}Al_{0.5-\delta}O_yN_{1-y}$ were calculated for y = 0, 0.125, 0.25, and 0.5 by energy minimization as a function of volume with the Birch-Murnaghan equation of states.[34] Within the isotropic approximation, bulk moduli were transformed to Young's moduli by

$$E = 3B(1 - 2\nu_S),$$

using the proportionality constant $3(1 - 2\nu_S) = 1.71$, to compare theoretical and experimental elastic modulus values. As mentioned in the experimental details, the Poisson's ratio of $\nu_S = 0.214$ is assumed to be independent of composition.[27]

Besides the substitution scenario where one N is replaced by exactly one O atom in $Ti_{0.5-\delta}Al_{0.5-\delta}O_yN_{1-y}$ ($\delta = 0$, referred to as 1:1 substitution in the following text), metal vacancies were introduced to counteract the oxygen incorporation-induced offset in charge balance (observed for the 1:1 substitution scenario) and rendering the metal vacancy containing structure charge neutral ($\delta \neq 0$, referred to as electroneutral configuration in the following text). The metal vacancy positions were chosen randomly. Based on Shaha *et al.*,[10] formal charges of +3, +3, −2, and −3 were assumed for Ti, Al, O, and N, respectively. These formal charges of the metals are motivated by charge neutrality considerations for the stoichiometric NaCl-structured nitride as discussed in detail in Ref. 10. The metal and non-metal sublattice atomic positions are shown in Fig. 1. For the 1:1 substitution scenario, Fig. 1(a), N as well as O populate all available non-metal sublattice positions; while in case of the electroneutral configuration, the local charge of the cell is balanced by formation of vacancies on the metal sublattice, Fig. 1(b). Bulk moduli and lattice parameters of $Ti_{0.5-\delta}Al_{0.5-\delta}O_yN_{1-y}$ for the electroneutral substitution ($\delta \neq 0$) with a non-integer amount of metal vacancies (e.g., 5.33 in case of y = 0.5) were obtained by linear interpolation (e.g., between 0 and 6 vacancies) and compared to the 1:1 substitution scenario.

IV. RESULTS AND DISCUSSION

A. Chemical composition

$(Ti_xAl_{1-x})_m(O_yN_{1-y})_n$ coatings with y in the range of 0 to 0.63 resulting in O concentrations ranging from 0 to 35 at. % were deposited by cathodic arc deposition. The Ti/(Ti + Al) ratio on the metal sublattice is $x = 0.61 \pm 0.01$ for all coatings and upon increasing O concentration the metal to non-metal ratio decreases from $m/n = 1.2$ to 0.8. The nitride coating exhibits a N concentration of 45 at. %. This understoichiometry is commonly observed in Ti-Al-N thin films,[1,35,36] and DFT calculations indicate that the formation of nitrogen vacancies is not only energetically favourable, but also that the calculated lattice parameters and elastic properties are consistent with experimental data.[27] Hence, the here obtained stress-free lattice parameter of the $(Ti_{0.61}Al_{0.39})_{0.55}N_{0.45}$ nitride with 4.165 Å (see Sec. IV B.) is in comparison to the calculated 4.20 Å for $Ti_{0.6}Al_{0.4}N$ (Ref. 32) consistent with the proposal of to Baben *et al.*[27]

$(Ti_xAl_{1-x})_m(O_yN_{1-y})_n$ coatings with y in the range of 0 to 0.88 resulting in O concentrations ranging from 0 to 54 at. % were deposited by HPPMS and the Ti/(Ti + Al) ratio is increased from x = 0.47 to 0.54, respectively, while the

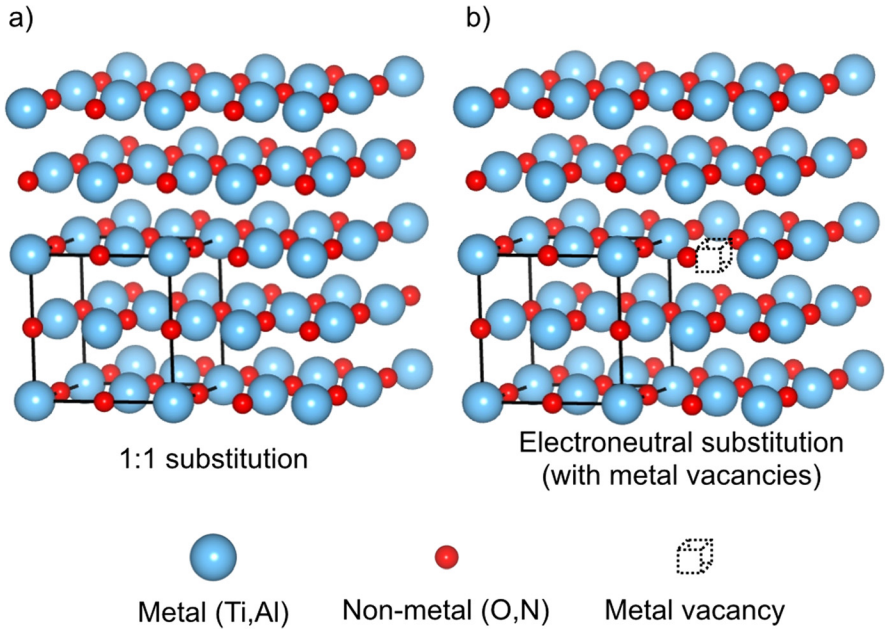

FIG. 1. Metal and non-metal sublattice positions of (Ti,Al) and (O,N), respectively, within the $Ti_{0.5-\delta}Al_{0.5-\delta}N_{1-y}O_y$ $2 \times 2 \times 2$ *ab initio* supercell for the (a) 1:1 substitution ($\delta = 0$) and (b) electroneutral substitution ($\delta \neq 0$) scenarios. The unit cell of NaCl-structured Ti-Al-O-N is emphasized by the solid line.

metal to non-metal ratio decreases from $m/n = 1.2$ to 0.6 upon increasing O concentration.

B. Structure

The structure evolution of arc-deposited Ti-Al-O-N coatings is deduced from a series of diffractograms for different O concentrations, presented in Fig. 2. The diffraction data for the HPPMS sputtered samples are given in Ref. 21. The data shown in Fig. 2 indicate the formation of a cubic solid solution for all samples investigated. Moreover, peaks with lower intensity at approximately 36.5° and 42.5° can be attributed to the TiN interlayer. The peaks at 45° and 65° belong to the steel substrate. A diffractogram of an uncoated substrate and a TiN interlayer deposited onto a steel substrate without Ti-Al-O-N top coating is supplied as reference.

For the coating without incorporated oxygen, the diffraction of the (111), (200), (220), and (311) lattice planes is consistent with the formation of a cubic $(Ti_{0.61}Al_{0.39})_{0.55}N_{0.45}$ solid solution. Upon oxygen incorporation, the intensity of all peaks is reduced. While the intensity decrease for (111), (220) and (311) peaks is strongest, the (200) diffraction signal is clearly visible, even for the $(Ti_{0.61}Al_{0.39})_{0.44}(O_{0.63}N_{0.37})_{0.56}$ coating containing the maximum O concentration, indicating a (200) texture. The formation of wurtzite AlN can be excluded for all Ti-Al-O-N coatings. As stated above, the diffraction data of the HPPMS coatings are reported elsewhere[21] and the evolution of a (200) texture was also observed. Since the authors observed indications for spinodal decomposition for O concentrations of approximately 39 at. % (Ref. 21), the concentration range utilized for the calculation of the lattice parameter was 0 to 35 at. %.

Stress-free lattice parameters of Ti-Al-O-N coatings were calculated from (111), (200), and (220) lattice planes and are shown in Fig. 3 as a function of O concentration. When the O concentration in the cathodic arc coatings is increased from 0 at. % ($(Ti_{0.61}Al_{0.39})_{0.55}N_{0.45}$) to 35 at. % ($(Ti_{0.61}Al_{0.39})_{0.44}(O_{0.63}N_{0.37})_{0.56}$), a decrease in lattice parameter values from 4.165 to 4.11 Å is observed. A similar decreasing trend is obtained for the HPPMS coatings: the lattice parameter value is reduced from 4.18 to 4.16 Å in an O concentration range from 18 at. % ($(Ti_{0.48}Al_{0.52})_{0.50}$ $(O_{0.35}N_{0.65})_{0.50}$) to 34 at. % ($(Ti_{0.50}Al_{0.50})_{0.45}(O_{0.61}N_{0.39})_{0.55}$).

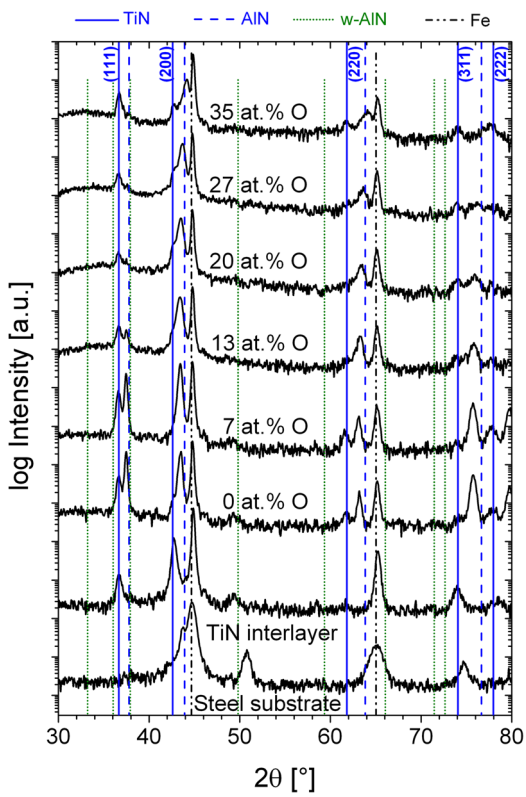

FIG. 2. Diffractogram of Ti-Al-O-N coatings, deposited by cathodic arc, compared for different O concentrations. Solid, dashed, and dotted lines are attributed to peak positions of cubic TiN, AlN, and wurtzite AlN, respectively. The dashed-dotted line indicates steel substrate peak positions. The coating compositions are $(Ti_{0.61}Al_{0.39})_{0.55}N_{0.45}$ (0 at.% O), $(Ti_{0.61}Al_{0.39})_{0.52}(O_{0.15}N_{0.85})_{0.48}$ (7 at.% O), $(Ti_{0.61}Al_{0.39})_{0.50}(O_{0.27}N_{0.73})_{0.50}$ (13 at. % O), $(Ti_{0.61}Al_{0.39})_{0.49}$ $(O_{0.39}N_{0.61})_{0.51}$ (20 at. % O), $(Ti_{0.61}Al_{0.39})_{0.47}(O_{0.51}N_{0.49})_{0.53}$ (27 at. % O), and $(Ti_{0.61}Al_{0.39})_{0.44}(O_{0.63}N_{0.37})_{0.56}$ (35 at. % O).

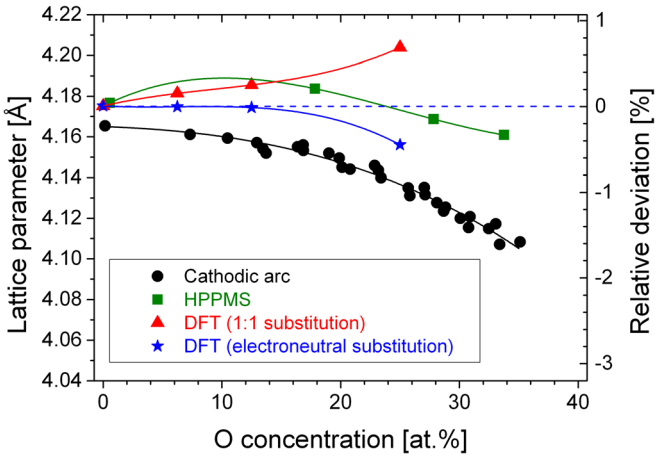

FIG. 3. Stress-free lattice parameters of Ti-Al-O-N coatings as a function of O concentration. Circles and squares represent lattice parameters of cathodic arc and HPPMS coatings, respectively. Triangles and stars represent lattice parameters of $Ti_{0.5-\delta}Al_{0.5-\delta}N_{1-y}O_y$, calculated by DFT for the 1:1 ($\delta = 0$) and electroneutral ($\delta \neq 0$) substitution, respectively. The 3rd order polynomial fits serve for estimation of the maximum deviation between experimental and computational data.

The lattice parameter values, calculated by DFT, are presented as well in Fig. 3 as a function of O concentration for the 1:1 substitution without metal vacancies and the electroneutral substitution with metal vacancies. The lattice parameter data of $Ti_{0.5-\delta}Al_{0.5-\delta}O_yN_{1-y}$ obtained by DFT depend significantly not only on the amount of incorporated oxygen but also on the metal sublattice population. The calculated results for configurations, where nitrogen is substituted by oxygen with a 1:1 ratio ($\delta = 0$, see 1:1 substitution, described in Sec. III) show increasing lattice parameters from 4.175 Å ($y = 0$) to 4.204 Å ($y = 0.5$) with increasing O concentration. This is consistent with previously published predictions,[7] but in conflict with the experimental data. However, for electroneutral configurations, where the presence of metal vacancies is considered ($\delta \neq 0$), the lattice parameter value decreases from 4.175 Å ($y = 0$) to 4.156 Å ($y = 0.5$) and is in excellent agreement with the stress-free lattice parameters of the here reported cathodic arc and HPPMS coatings: The maximum deviation between the measured stress-free lattice parameters of coatings deposited by cathodic arc and HPPMS and the DFT data is 0.5% and 0.4%, respectively (Fig. 3). These deviations are below the accuracy limit of *ab initio* lattice parameter calculations.[37] Hence, the here presented data strongly support that the notion put forward by Shaha *et al.*[10] for sputtered V-Al-O-N is also relevant for Ti-Al-O-N: charge balancing[13] is enabled by the oxygen incorporation-induced formation of metal vacancies and this physical mechanism appears to be equally relevant for Ti-Al-O-N and V-Al-O-N and, hence, may be of relevance for cubic transition metal aluminium oxynitrides in general. Furthermore, the formation of metal vacancies is observed during sputter deposition and during cathodic arc deposition of Ti-Al-O-N coatings.

C. Elastic properties

Next, we discuss the relevance of the formation of metal vacancies in Ti-Al-O-N for the elastic properties. The surface roughness of the coatings was measured by laser microscopy. Cathodic arc coatings with thickness values of approximately 3 μm exhibit average roughness values in the range of 50 to 90 nm, while the coatings deposited by HPPMS with thickness values of approximately 1 μm show average roughness values <10 nm.

Young's moduli of Ti-Al-O-N coatings were measured by nanoindentation and are presented in Fig. 4 as a function of O concentration. The Young's modulus values of cathodic arc coatings decrease from 553 ± 117 to 342 ± 59 GPa upon increasing O concentration from 0 at. % $((Ti_{0.61}Al_{0.39})_{0.55}N_{0.45})$ to 35 at. % $((Ti_{0.61}Al_{0.39})_{0.44}(O_{0.63}N_{0.37})_{0.56})$. The same trend is valid for the phase pure cubic HPPMS coatings: Young's modulus values decrease from 449 ± 17 to 320 ± 11 GPa for O concentrations from 0 at. % $((Ti_{0.47}Al_{0.53})_{0.55}N_{0.45})$ to 34 at. % $((Ti_{0.50}Al_{0.50})_{0.45}(O_{0.61}N_{0.39})_{0.55})$, respectively. Hence, the elastic modulus of phase pure cubic Ti-Al-O-N coatings is reduced by up to 35% for O concentrations >30 at. %. However, the scattering of Young's modulus values is larger for the cathodic arc coatings as compared to the sputtered coatings. This is attributed to the significantly larger surface roughness which has to be expected for coatings grown by unfiltered cathodic arc deposition.[38] With a deviation of $<15\%$, very good agreement between Young's moduli of coatings deposited by cathodic arc and HPPMS is obtained. The reduction in elastic modulus is, therefore, defined by the concentration of incorporated oxygen and not by the deposition technique or synthesis pathway.

Furthermore, bulk moduli were obtained by DFT calculations and used to calculate Young's moduli for $Ti_{0.5-\delta}Al_{0.5-\delta}O_yN_{1-y}$ with $y = 0$, 0.125, 0.25, and 0.5, shown in comparison to the above discussed experimental data in Fig. 4. The same trend of decreasing elasticity as a function of O concentration is obtained from DFT calculations for $Ti_{0.5-\delta}Al_{0.5-\delta}O_yN_{1-y}$: Young's modulus values in case of the 1:1 substitution ($\delta = 0$, without metal vacancies) decrease from 456 GPa ($y = 0$) to 372 GPa ($y = 0.5$) consistent with previous reports.[7] If metal vacancies are considered

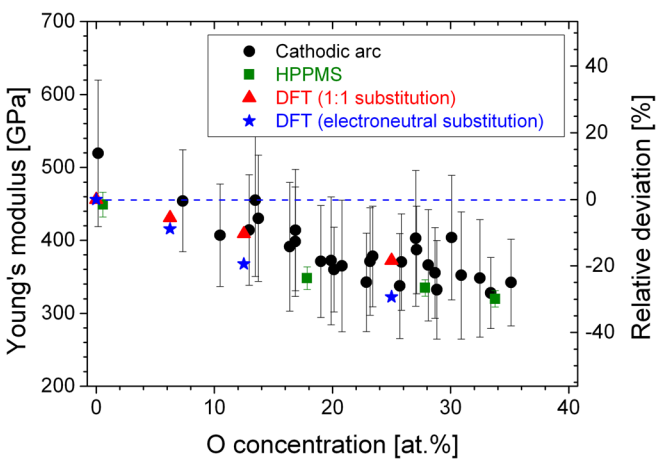

FIG. 4. Young's modulus of Ti-Al-O-N coatings as a function of O concentration. Circles and squares indicate Young's moduli of cathodic arc and HPPMS coatings, respectively. Triangles and stars represent Young's moduli of $Ti_{0.5-\delta}Al_{0.5-\delta}N_{1-y}O_y$, calculated by DFT for the 1:1 ($\delta = 0$) and electroneutral ($\delta \neq 0$) substitution, respectively.

in the electroneutral substitution scenario ($\delta \neq 0$), Young's modulus values decrease from 456 GPa ($y = 0$) to 322 GPa ($y = 0.5$). The deviation between experimental and calculated Young's moduli is with <15% very good.

From these data, two causes for the observed reduction of Young's modulus upon oxygen incorporation can be identified: First, oxygen incorporation-induced metal vacancy formation results in a reduction in elasticity. Second, the formation of, compared to the metal nitrogen bonds, relatively weak metal oxygen bonds as proposed by to Baben *et al.*[7] and Rotert *et al.*[8] We have demonstrated here that both effects act in an additive manner.

Furthermore, taking these mechanisms into account, the effect on reduction in elasticity may be estimated separately, based on the DFT data. Comparing $Ti_{0.5-\delta}Al_{0.5-\delta}O_{0.5}N_{0.5}$ to $Ti_{0.5-\delta}Al_{0.5-\delta}N$ for the 1:1 substitution ($\delta = 0$), the Young's modulus is reduced by 18% and additionally by 11% for the electroneutral substitution ($\delta \neq 0$). Hence, it is evident that oxygen incorporation promotes metal vacancy-induced reduction in elasticity and formation of weak Ti-O and Al-O bonds in the same order of magnitude.

V. CONCLUSIONS

Ti-Al-O-N coatings with cubic solid solution structure were deposited by cathodic arc and HPPMS with a broad O concentration range of 0 to 35 at. % and 0 to 34 at. %, respectively. The stress-free lattice parameter of the coatings exhibited a decreasing trend upon increasing O concentration. The agreement between experimental and theoretical lattice parameter data was excellent with deviations <1%. DFT calculations revealed that the oxygen incorporation-induced formation of metal vacancies enables charge balancing. The Young's modulus of Ti-Al-O-N cathodic arc and HPPMS coatings was found to decrease by up to 35%, when the O concentration is increased from 0 to 35 and 34 at. %, respectively, and the deviation between experimental results and DFT calculations was with <15% in very good agreement. The reduction in elasticity is driven by two additive acting contributions: First, the formation of metal vacancies and second, the formation of relatively weak metal oxygen bonds, compared to the corresponding metal nitride bonds. Furthermore, it was shown that the evolution of structural and mechanical properties of Ti-Al-O-N coatings depends on the chemical composition only and not on the deposition technique. By comparison with previously published predictions by Rotert *et al.*[8] and Shaha *et al.*,[10] we suggest that the notion of charge balancing due to metal vacancy formation and formation of relatively weak metal oxygen bonds are generally valid for the incorporation of oxygen into cubic transition metal aluminium nitrides.

ACKNOWLEDGMENTS

This work was supported by Deutsche Forschungsgemeinschaft within the Collaborative Research Center SFB-TR 87/2 "Pulsed high power plasmas for the synthesis of nanostructured functional layers."

[1]W.-D. Münz, J. Vac. Sci. Technol. A **4**, 2717 (1986).
[2]P. H. Mayrhofer, R. Rachbauer, F. Rovere, D. Holec, and J. M. Schneider, in *Comprehensive Materials Processing*, edited by M. S. J. Hashmi (Elsevier, Ltd., Oxford, UK, 2014), p. 355.
[3]K. Tönshoff, B. Karpuschewski, A. Mohlfeld, T. Leyendecker, G. Erkens, H. G. Fuß, and R. Wenke, Surf. Coat. Technol. **108–109**, 535 (1998).
[4]K. Kawata, H. Sugimura, and O. Takai, Thin Solid Films **390**, 64 (2001).
[5]J. Sjölén, L. Karlsson, S. Braun, R. Murdey, A. Hörling, and L. Hultman, Surf. Coat. Technol. **201**, 6392 (2007).
[6]A. Hörling, L. Hultman, M. Odén, J. Sjölén, and L. Karlsson, Surf. Coat. Technol. **191**, 384 (2005).
[7]M. to Baben, L. Raumann, and J. M. Schneider, J. Phys. D: Appl. Phys. **46**, 084002 (2013).
[8]S. J. Rotert, D. Music, M. to Baben, and J. M. Schneider, J. Appl. Phys. **113**, 083512 (2013).
[9]H. Najafi, A. Karimi, P. Dessarzin, and M. Morstein, Thin Solid Films **520**, 1597 (2011).
[10]K. P. Shaha, H. Ruess, S. J. Rotert, M. to Baben, D. Music, and J. M. Schneider, Appl. Phys. Lett. **103**, 221905 (2013).
[11]F. Mei, Y. Dong, Y. Li, and G. Li, Mater. Lett. **60**, 375 (2006).
[12]L. Castaldi, D. Kurapov, A. Reiter, V. Shklover, P. Schwaller, and J. Patscheider, Surf. Coat. Technol. **203**, 545 (2008).
[13]L. Pauling, J. Am. Chem. Soc. **51**, 1010 (1929).
[14]J. M. Schneider, B. Hjörvarsson, X. Wang, and L. Hultman, Appl. Phys. Lett. **75**, 3476 (1999).
[15]S. G. Ebbinghaus, H.-P. Abicht, R. Dronskowski, T. Müller, A. Reller, and A. Weidenkaff, Prog. Solid State Chem. **37**, 173 (2009).
[16]R. Marchand, Y. Laurent, J. Guyader, P. L'Haridon, and P. Verdier, J. Eur. Ceram. Soc. **8**, 197 (1991).
[17]A. Pélisson, M. Parlinska-Wojtan, H. J. Hug, and J. Patscheider, Surf. Coat. Technol. **202**, 884 (2007).
[18]C. A. Pignedoli, D. Passerone, H. J. Hug, A. Pélisson-Schecker, and J. Patscheider, Appl. Phys. Lett. **96**, 071908 (2010).
[19]A. Khatibi, J. Sjölén, G. Greczynski, J. Jensen, P. Eklund, and L. Hultman, Acta Mater. **60**, 6494 (2012).
[20]A. Khatibi, J. Palisaitis, C. Höglund, A. Eriksson, P. O. Å. Persson, J. Jensen, J. Birch, P. Eklund, and L. Hultman, Thin Solid Films **519**, 2426 (2011).
[21]C. Gnoth, C. Kunze, M. Hans, M. to Baben, J. Emmerlich, J. M. Schneider, and G. Grundmeier, J. Phys. D: Appl. Phys. **46**, 084003 (2013).
[22]Y. W. Zhang, H. J. Whitlow, T. Winzell, I. F. Bubb, T. Sajavaara, K. Arstila, and J. Keinonen, Nucl. Instrum. Methods Phys. Res. B **149**, 477 (1999).
[23]M. S. Janson, CONTES Instruction Manual Uppsala, Internal Report (2004).
[24]C. Genzel, Phys. Status Solidi A **159**, 283 (1997).
[25]F. Tasnádi, I. A. Abrikosov, L. Rogström, J. Almer, M. P. Johansson, and M. Odén, Appl. Phys. Lett. **97**, 231902 (2010).
[26]W. C. Oliver and G. M. Pharr, J. Mater. Res. **7**, 1564 (1992).
[27]M. to Baben, L. Raumann, D. Music, and J. M. Schneider, J. Phys.: Condens. Matter **24**, 155401 (2012).
[28]P. Hohenberg and W. Kohn, Phys. Rev. **136**, B864 (1964).
[29]J. P. Perdew and W. Yue, Phys. Rev. B **33**, 8800 (1986).
[30]H. J. Monkhorst and J. D. Pack, Phys. Rev. B **13**, 5188 (1976).
[31]P. E. Blöchl, O. Jepsen, and O. K. Andersen, Phys. Rev. B **49**, 16223 (1994).
[32]P. H. Mayrhofer, D. Music, and J. M. Schneider, J. Appl. Phys. **100**, 094906 (2006).
[33]A. Zunger, S.-H. Wei, L. G. Ferreira, and J. E. Bernard, Phys. Rev. Lett. **65**, 353 (1990).
[34]F. Birch, J. Geophys. Res. **83**, 1257, doi:10.1029/JB083iB03p01257 (1978).
[35]A. Hörling, L. Hultman, M. Odén, J. Sjölén, and L. Karlsson, J. Vac. Sci. Technol. A **20**, 1815 (2002).
[36]J. Bujak, J. Walkowicz, and J. Kusinski, Surf. Coat. Technol. **180–181**, 150 (2004).
[37]J. Paier, M. Marsman, K. Hummer, G. Kresse, I. C. Gerber, and J. G. Ángyán, J. Chem. Phys. **124**, 154709 (2006).
[38]A. Anders, *Cathodic Arcs* (Springer, New York, NY, 2008), pp. 265–268.